Vapor growth of semiconducting P allotropes into TiO_2 nanotube arrays for photo-electrocatalytic water splitting applications

Journal:	*ACS Applied Nano Materials*
Manuscript ID	an-2019-00221s
Manuscript Type:	Article
Date Submitted by the Author:	05-Feb-2019
Complete List of Authors:	Üzer, Ebru; Technische Universitat Munchen, Chemistry Kumar, Pawan; University of Alberta Faculty of Engineering, Department of electrical and Computer Engineering Kisslinger, Ryan; University of Alberta Faculty of Engineering, Department of electrical and Computer Engineering Kar, Piyush; University of Alberta, Shankar, Karthik; University of Alberta, Electrical & Computer Engineering Nilges, Tom; Technische Universität München , Chemistry

Vapor growth of semiconducting P allotropes into TiO_2 nanotube arrays for photo-electrocatalytic water splitting applications

Ebru Üzer,[a] Pawan Kumar,[b] Ryan Kisslinger,[b] Piyush Kar,[b] Karthik Shankar,[b,] and Tom Nilges[a,*]*

Department of Chemistry, Technical University of Munich, Lichtenbergstr. 4, 85748 Garching, Germany; E-mail: tom.nilges@lrz.tum.de

Department of Electrical and Computer Engineering, 9211-116 Street NW, Edmonton, Alberta, Canada T6G 1H9; E-mail: kshankar@ualberta.ca.

KEYWORDS. Phosphorus, TiO_2, vapor phase deposition, low band gap materials, photocatalyst, heterojunction, Sunlight driven water splitting.

ABSTRACT. Recent evidence of exponential environmental degradation will demand a drastic shift in research and development towards exploiting alternative energy resources such as solar energy. Here, we report the successful low-cost and easily accessible synthesis of hybrid semiconductor@TiO_2 nanotube photocatalysts. In order to realize its maximum potential in harvesting photons in the visible light range, TiO_2 nanotubes have been loaded with earth

abundant, low band gap fibrous red P and black P. SEM-, STEM-EDS, XRD, Raman spectroscopy, XPS and UV-Vis measurements have been performed, substantiating the deposition of fibrous red- and black P on top and inside the cavities of 100 µm long electrochemically fabricated nanotubes. The nanotubular morphology of titania and a vapor transport technique is utilized to form heterojunctions of P and TiO_2. Compared to pristine anatase 3.2 eV-TiO_2 nanotubes, the creation of heterojunctions in the hybrid material resulted in 1.5 – 2.1 eV photoelectrocatalysts. An enhanced photoelectrochemical water splitting performance under visible light compared with the individual components resulted for the phosphorus@TiO_2 hybrids. This feature is due to synergistically improved charge separation in the heterojunction and more effective visible light absorption. The electronic band structure and charge carrier dynamics are investigated in detail to elucidate the charge separation mechanism. A Fermi level alignment in phosphorus@TiO_2 heterojunctions leads to a more reductive flat band potential and a deeper valence band compared to pristine phosphorus, and thus facilitate better water splitting performance. Our results demonstrate effective conversion efficiencies for the nanostructured hybrids that may enable future applications in optoelectronic applications such as photodetectors, photovoltaics, photoelectrochemical catalysts and sensors.

INTRODUCTION

Limited reserves of carbon-emitting fossil fuels and their associated negative environmental impact have triggered research to find alternative self-sustainable technologies. Sunlight driven water splitting to generate hydrogen fuels is a promising approach as an alternate energy technology. However, photo-splitting of water to generate

hydrogen is unfavorable due to a high positive Gibbs free energy change (+237 kJ mol^{-1}), and the process requiring a photocatalyst (usually semiconductor) with appropriate conduction band (CB) and valence band (VB) positions.[1] Various nanostructured semiconductor materials have been extensively investigated for application in photochemical and photoelectrochemical water splitting *i.e.* $BiVO_4$, WO_3, Fe_2O_3, MoS_2, CoO, g-C_3N_4, CdS, $Ga_{1-x}Zn_xN_{1-x}O_x$, SnS_2 and $SrTiO_3$ *etc.*[2-7] However, meeting the broad range of required properties in one single material to actuate water splitting remains a challenge; such properties include visible light absorptivity, long lived charge carriers, high quantum efficiency, electrochemical resiliency, low-cost and non-toxicity with appropriateness of conduction (<0.00 V *vs* NHE) and valence band edges (>1.23 V *vs* NHE) for electron transfer and formation of hydrogen (reduction) and oxygen from water (oxidation) respectively. TiO_2, which meets many of the aforementioned requirements, nevertheless suffers from poor visible light absorption and fast recombination of photogenerated charge carriers. Band structure manipulation of TiO_2 *via* approaches such as doping, sensitization, heterojunction formation *etc.* and morphological engineering are enticing approaches to improve the quantum efficiency.[8-11] One dimensional TiO_2 nanostructures like nanorods, nanotubes, nanocones *etc.* are particularly interesting due to their large accessible surface area, vectorial charge transport pathways and a carrier retrieval length comparable to the smallest dimension of the nanostructure. Thus, they have emerged as excellent candidates for heterojunction formation with low band gap semiconductors.[12-17]

Low-cost TiO_2 nanotube layers fabricated *via* electrochemical anodization present varied applications in photocatalytic, photovoltaic and optoelectronic sensing devices.[18-20] By

maximizing the specific surface area from bulk to nanoparticulate TiO_2, improvement of in photoelectrochemical water splitting performance using solar light can be achieved.[21] To broaden the application spectrum and overcome key drawbacks of TiO_2 nanotubes, our intention is band gap engineering and semiconductor/electrolyte contact optimization, which play a major role in efficient photocatalytic water splitting.[22-23] Therefore, we utilize a hybrid system of semiconductor materials between highly ordered self-organized TiO_2 nanotube membranes and inexpensive phosphorus allotropes, 1D fibrous red P and 2D black P, which leads to higher efficiency composite photocatalysts. As-prepared hollow nano-sized cylinders of TiO_2 nanotubes, were formed by electrochemical, field aided, three-step anodization of Ti films or foils in electrolytes containing $F^-/I^-/ClO_3^-$ ions. Both phosphorus allotropes were deposited *via* low pressure chemical vapor deposition.[24-25] In order to prevent the semiconductor-semiconductor hybrid from material degradation during long thermal treatment processes, the vapor deposition or so-called mineralization technique allows crystallization of amorphous TiO_2 to anatase. At the same time, desirable growth of phosphorus nanorods inside and onto the nanotubes in one annealing step (at ~500 °C) takes place. The intrinsic band gap for the *n*-type semiconductor anatase TiO_2 in the UV range at 3.2 eV limits light absorption to only < 5 % of the solar spectrum.[26] To exploit the solar spectrum much better, heterojunction systems with two phosphorus allotropes were investigated: a) fibrous red P, exhibiting a band gap of 2.25 eV based on our experimental results and b) *p*-type semiconducting black P, owing a direct bandgap of 0.3 eV for bulk material in the near IR region. The latter is characterized by a high, layer dependent hole carrier mobility of ca. 10^5 cm^2/Vs.[27-29] Fibrous red P is being investigated regarding its potential as water splitting agent and black P as field effect transistor,

photodetector and sensor.[30-32] In a heterojunction system, the photogenerated carrier mechanism can induce the formation of a built-in potential (V_{bi}) and hinder electron hole pair recombination.[33-36] The dense hybrid structure supports fast charge separation of carriers, created inside the nanorods and migration of a short distance equal to the nanotube radius to cross the heterojunction interface. Excellent quantum yields can be obtained from the suitable nanotube structure, owing to a high aspect ratio, which ensures efficient photon harvesting, orthogonalized processes of charge separation and light absorption, and improved light trapping by Mie scattering.[37-39] Modification of TiO_2 nanotubes has been approached by decoration of surfaces with noble metal nanoparticles, such as Au, Ag, and Pt. A solid interface occurs, where a Schottky-contact is formed that is less preferable than a p/n-semiconductor contact in terms of charge carrier recombination loss.[23, 38, 40-41] Recently, desired Z-scheme junction formation has been successfully carried out with CdS, g-C_3N_4, MoS_2, $ZnIn_2S_4$, Fe_2O_3, halide perovskites *etc*. for use in extensive photocatalytic applications such as CO_2 photoreduction, high performance photoanodes for water splitting devices, selective gas sensors, and high efficiency solar cells.[42-47] In this work we introduce a vapor transport process to grow hybrid semiconductor-semiconductor 1D and 2D materials to form heterojunctions, capable of realizing enhanced photoelectrochemical water splitting.

RESULTS AND DISCUSSION

This section is divided into two main chapters: Structural characterization of fibrous red P- and black P deposited into and onto the TiO_2 nanotube arrays and the photocatalytic activity of the phosphorus allotrope@TiO_2 hybrid materials. Spectroscopic (XPS studies in Supporting information, UV-vis and Raman) and diffraction experiments (XRD as

Supporting Information) were applied to characterize the bare and hybrid materials. A brief photo-electrocatalytic investigation, of the phosphorus allotrope@TiO_2 hybrid materials contains the full electrochemical characterization including a plausible mechanism for the water splitting activity of the title compounds.

Structural Characterization of phosphorus allotrope@TiO_2 nanotube hybrids

In order to fabricate hybrid semiconducting materials, we succeeded in filling the anatase-type TiO_2 nanotubes with fibrous red phosphorus and black phosphorus using a short-way transport reaction (Figure 1, experimental details are given in the Supporting Information). This reaction is adapted from the so-called mineralization-principle used for the synthesis of a plethora of phosphorus containing compounds, as in fibrous P solely, binary and ternary phosphorus compounds like NaP_7 and SnIP.[48-50]

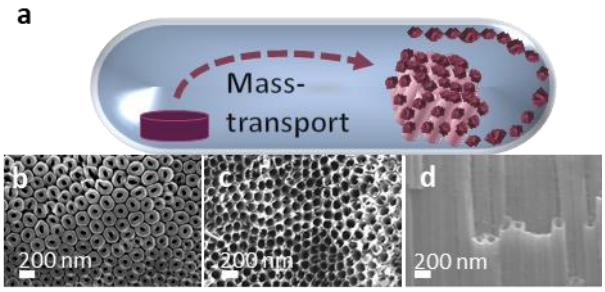

Figure 1. a) Here, fibrous phosphorus (purple pellet) is reacted onto and into TiO_2 nanotube membranes (pink). **b)** Representative SEM pictures of the electrochemically-prepared TiO_2 nanotube membranes used in a mineralizer-driven short-way transport reaction in bottom side view, **c)** top side view, **d)** side view.

The TiO_2 nanotube structure could be preserved after deposition of the phosphorus allotropes via thermal treatment during the transport reactions.

Fibrous red P@TiO_2 nanotubes. The mineralization method can be applied to prepare element allotropes, binary compounds and ternary compounds. An example is the successful deposition

of fibrous red P onto and into TiO_2 nanotube membranes *via* gas phase as shown in Figure 2. Pure fibrous P exhibits photocatalytic activity and has potential for water splitting applications.[20] Fibrous red P has been formed everywhere on the TiO_2 nanotube membrane (see Figure 2b). Noticeably, fibrous P is distributed on the whole surface of the membranes as SEM-EDS measurements exhibited in Figure 2c, d, and Table S1. According to powder X-ray diffraction data, the growth of fibrous red P on top of the TiO_2 nanotube membranes was confirmed (Figure S1).

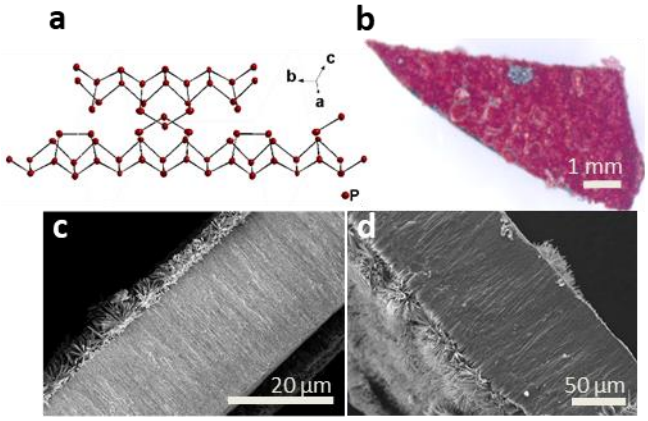

Figure 2. a) Crystal structure of fibrous red P. **b)** A TiO_2 nanotube membrane covered with fibrous red P after reaction *via* gas phase. **c)** and **d)** SEM images of the cross section and surface of fibrous P@TiO_2 nanotube membranes. Fibrous P covering the surface of the membrane. EDS of the cross section show phosphorus all along the nanotubes (Table S1).

STEM images taken after separation of the TiO_2 nanotubes by an ultrasonication process show a ranged bundle of nanotubes with a diameter of ~90-100 nm. Elemental mapping confirms Ti, O and P with a distribution of P along the full tube lengths (see Figure 3).

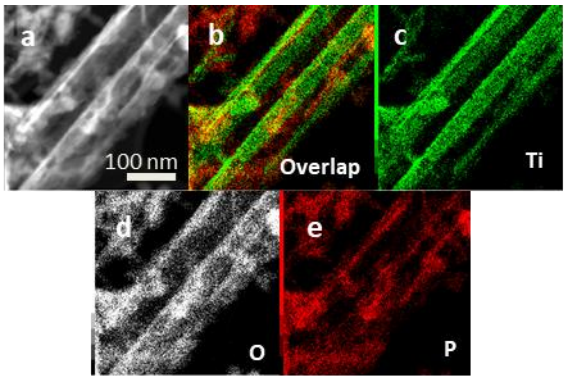

Figure 3. a) STEM bright-field image of TiO_2 nanotubes separated from a membrane by an ultrasonication procedure. **b)** Elemental mapping of overlaid elements Ti, O and P. **c)** and **d)** Ti and O of the TiO_2 nanotubes, with **e)** P distributed along the full length of the tubes.

A successful growth of the fibrous red P structure up to a certain depth into the TiO_2 nanotube arrays can be verified *via* Raman measurements. Therefore, TiO_2 nanotube membranes were cut along the cross section after chemical vapour deposition of fibrous red P and imaging at specific spots from the surface of a TiO_2 nanotube array downwards along a vertical line was acquired. The laser has a standard mode spot size of 1.5 micron (at 50x magnification). Raman spectra were recorded at several spots along the 65 µm long cross section of the membranes. The experimental frequencies of bulk fibrous red P match the significant modes between 352 and 462 cm^{-1} recorded up to 20 □m in distance to the surface from top side and 15 □m in distance to the surface from bottom side along the cross section of the membranes (shown in Figure S2). A systematic detection of spots further into the 65 µm long tubes show the expected modes for pure anatase and the additional characteristic modes of fibrous P up to 15 µm recorded from the top side of the nanotube array and 15 µm from the bottom side (see Figure 4). A reduction of crystallinity of fibrous red P as going deeper into the tubes can be observed.

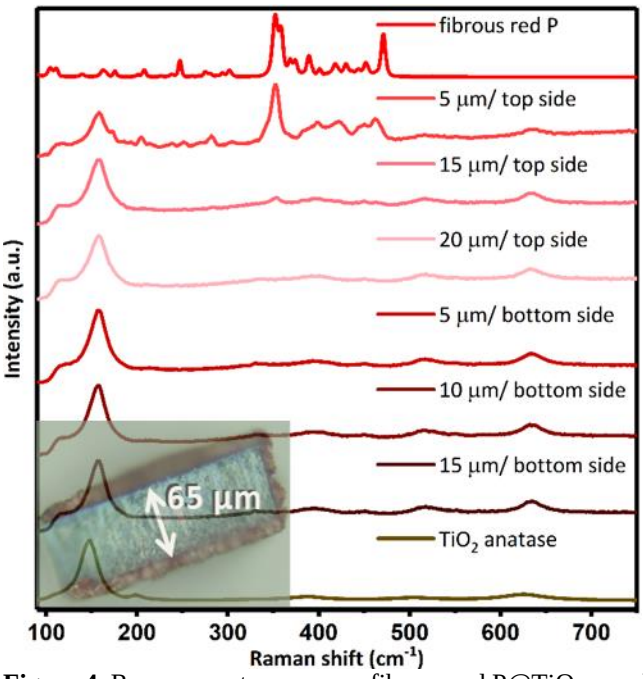

Figure 4. Raman spectroscopy on fibrous red P@TiO_2 membranes. From top to down: Reference Raman spectrum of fibrous red P, spectra of a fibrous red P@TiO_2 membrane cross section measured at approx. 5, 15 and 20 µm in distance to the surface (membrane-top side), at approx. 5, 10 and 15 µm in distance to the surface (membrane-bottom side) and a blank TiO_2 membrane (anatase, brown).

After successful growth of fibrous red phosphorus onto and into TiO_2 nanotube arrays was demonstrated *via* Powder X-ray diffraction, SEM-EDS, Raman spectroscopy and STEM-EDS analysis. A growth of partially crystalline fibrous P into the membrane was realized, whereas nicely crystalized fibrous P was found at the surface of the membranes.

Black P@TiO_2 nanotubes. A similar successful gas-phase deposition has been performed with black P, another element allotrope of phosphorus. Black P is characterized by a structure (No. of neighboured phosphorus layers) dependent band gap value covering a wide range of the electromagnetic spectrum.[51] Thus, black phosphorus has potential in applications such as field-effect transistors, *p-n* junctions, photodetectors etc.[52] This orthorhombic allotrope of phosphorus crystallizes in space group *Cmca* (crystal structure

in Figure 5a), shows a high carrier mobility and in-plane anisotropy, playing a role in hydrogen and oxygen generation in photocatalytic water-splitting.[51] Moreover, a broadening of the absorption fraction towards the visible light range of 3.2 eV-TiO_2 anatase can be provided by a heterojunction formation with the narrow band gap semiconductor black P. Dependent on the number of neighbouring layers stacked onto each other, a band gap of 0.3 eV in bulk black P to ~2 eV for the monolayer (called phosphorene) can be realized. The overall efficiency of existing narrow band gap water-splitting photocatalysts is affected by photocorrosion, which results from chemical bond strength of the given system.[53] This fact can be avoided by fabrication of a heterojunction hybrid system between black P and TiO_2 nanotube arrays, where the chemical bond strength of the bulk material (TiO_2 anatase) will remain and only an alignment of Fermi levels between the materials during charge carrier transport reactions within the hybrid occurs.[23] A visual deposition of characteristic flat metallic coloured needles, spreading out gradually on the TiO_2 nanotube membranes (reversed side) can be seen in Figure 5b. A SEM image in Figure5b shows the successful deposition of a thick black P layer covering the surface of this cut cross section part of a TiO_2 nanotube membrane. The second SEM image in Figure 5d is displaying a gradual growth of small horizontally aligned black P crystals in between the two arrows, which is confirmed by EDX-measurements (Table S2). A reason of this unusual growth can be the unique 2D structure of black P. Powder X-ray diffraction data, can confirm the formation of black P on top of the TiO_2 nanotube arrays (Figure S3).

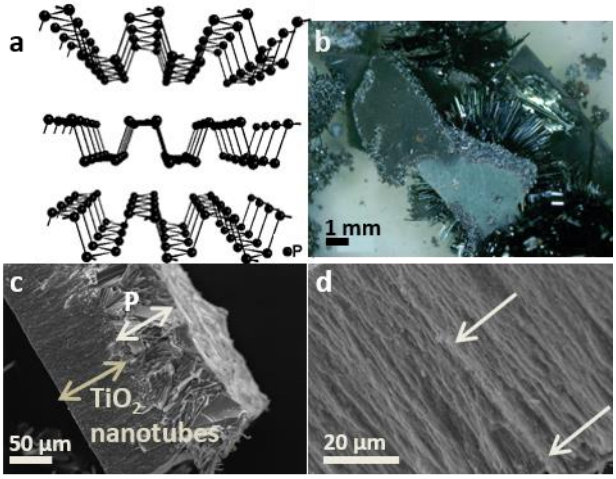

Figure 5. a) Crystal structure of black P. **b)** TiO_2 nanotube membranes with black P needles on front and backside after reaction *via* gas phase. **c)** and **d)** SEM images of cross section and covered surface of black P@TiO_2 nanotube membranes. Visible horizontal growth along vertical tube axis between white arrows. EDS of the cross section show phosphorus all along the nanotubes.

After separation of the TiO_2 nanotubes in an ultrasonication process, STEM imaging displays a singular tube with the width of ~150 nm. Phosphorus was detected inside the tube besides Ti from the TiO_2 membrane after elemental mapping. Furthermore, analysis of Sn and I inside the tubes was carried out due to the fact that SnI_4 was used during the transport reaction during synthesis. The formation of SnIP, as possible side product in such a transport reaction was ruled out (see Figure 6).[50]

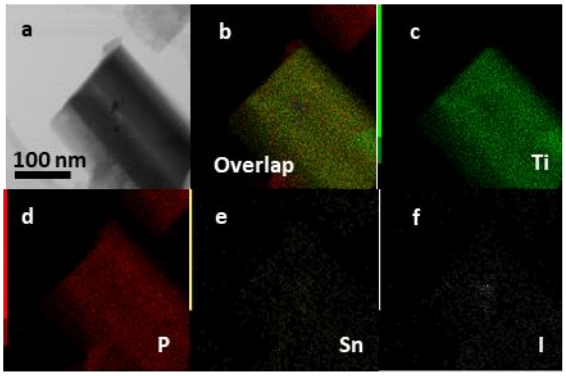

Figure 6. a) STEM bright-field image of TiO_2 nanotubes separated from a membrane by an ultrasonication procedure. **b)** Elemental mapping of overlaid elements Ti (representing TiO_2), P, Sn and I. **c)** Ti and **d)** P substantiating P

distributed along the full length of a TiO_2 nanotube with **e)** Sn and **f)** I coming from the mineralizer is only present in small amounts.

To verify the successful growth of black P into TiO_2 nanotubes, several Raman spectra were recorded after cutting the nanotube membranes at the cross section after synthesis. A simultaneous presence at the membrane surface of black P (main phase) with the most prominent modes at 360 cm^{-1}, 436 cm^{-1} and 464 cm^{-1} next to anatase with a characteristic mode at 145 cm^{-1} can be confirmed. A gradual change is detectable, when pointing the laser down to a depth of 7 µm into the nanotubes, were black P next to anatase (main phase) still can be confirmed, see Figure 7. The crystallinity of the black P phase remains unchanged, in comparison to Raman imaging of fibrous red P@TiO_2 nanotubes. This is an additional proof of the assumption of distinct P-needles in the SEM image in Figure 5d.

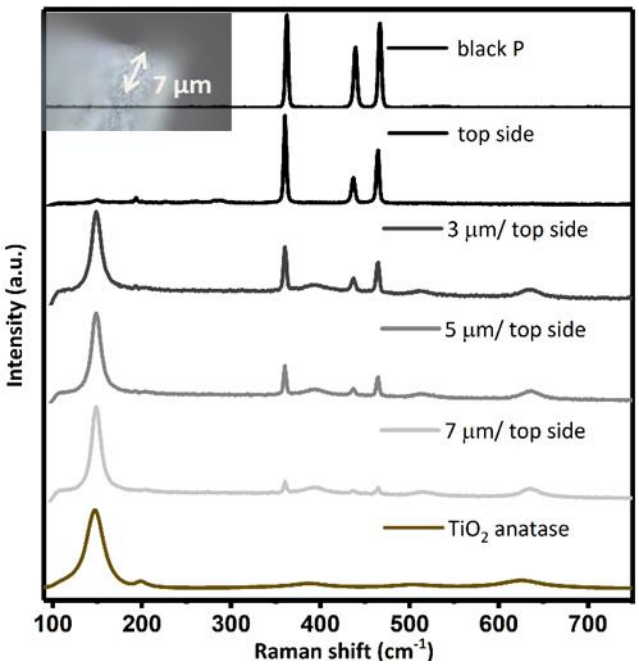

Figure 7. Raman spectroscopy on black P@TiO_2 membranes. From top to down: Reference Raman spectrum of black P, spectra of a black P@TiO_2 membrane cross section measured at the surface and approx. 3, 5, and 7 µm in distance to the surface (membrane-top side), and a fresh TiO_2 membrane (anatase, brown).

XPS Spectroscopy. The characterization of surface composition, binding energies and oxidation states of fibrous red P and black P next to blank TiO_2 samples, hybrid fibrous red P@TiO_2 and black P@TiO_2 were investigated *via* high resolution-XPS studies. The heterostructure systems reveal consistent oxidation states along with the pure samples. A shift of binding energies in the O1s region of fibrous red P@TiO_2 and black P@TiO_2 compared to pristine TiO_2 can be primarily attributed to a formation of P-O bonds in the heterostructure system (Figure S5 and S6).

UV-Vis spectroscopy. The optical properties of the samples were determined using UV-Vis in diffuse reflectance mode (Figure S4). A sharp peak around 320 nm in the UV-Vis spectrum of TiO_2 with a band tailing up to 380 nm arises from O2p→Ti3d transition of electrons demonstrating valence band to conduction band transition. The absorption spectrum of fibrous red P show a broad absorption band extending to the visible range. Fibrous red P deposited on wide bandgap TiO_2 shows improved absorption in visible region due to presence of moderate bandgap fibrous red P. The UV-Vis spectrum of black P shows three absorption bands at 315, 374 and 438 nm with broadening of absorption bands in the IR region. This is in line with findings in the published literature.[54-55] After deposition of black P on TiO_2 nanotubes, the visible light and IR absorption range was increased which demonstrates better visible light response of samples.

Visible light absorption of the samples was investigated in detail using Tauc plots, by plotting a graph between $(\alpha h\nu)^{1/2}$ *vs* $h\nu$ followed by extrapolation of a linear tangent to the X-axis; where α is the absorption coefficient, h is the plank constant and ν is the light frequency (Figure S4). The values of the optical band gaps from the Tauc plots were found to be 2.97 eV for TiO_2, 1.97 eV for fibrous red P, 2.1 eV for fibrous red P@TiO_2, 1.67 eV

for black P and 1.54 eV for black P@TiO_2 respectively which were in close agreement with reported values and clearly demonstrate absorption in the visible region by the heterojunction hybrids (Figure S4).

Photocatalytic activity of phosphorus allotrope@TiO_2 nanotube hybrids

The performance in photo-electrochemical water splitting of all compounds was tested using a three-electrode system. In this setup, the specimens, deposited on FTO, formed the anode (working electrode) while Pt and Ag/AgCl were used as cathode (counter electrode) and reference electrode respectively. The photoanode was irradiated with AM1.5 G simulated sunlight with a power density of 100 mW cm^{-2} (one sun) at the sample surface. The current density in mA cm^{-2} was measured using linear sweep voltammetry (LSV) by sweeping the applied voltage from -0.1 V to +0.8 V *vs* Ag/AgCl at a scan rate of 0.1 V s^{-1}. To compare the photo response, dark current was also measured. The photocurrent response during light On-Off cycles shows a rise and drop in photocurrent which substantiates the photogeneration of charge carriers in the samples under light irradiation (Figure 8a and b). The photocurrent densities for TiO_2, fibrous red P, fibrous red P@TiO_2, black P and black P@TiO_2, at 0.6 V *vs* Ag/AgCl (1.23 V *vs* RHE; water oxidation potential) were measured to be 0.22, 0.25, 0.60, 0.19 and 0.20 mA cm^{-2} respectively (Figure 8c). Under dark condition, negligible current was observed. The photocurrent densities of pristine black P, bare TiO_2 and pristine fibrous red P were almost identical due to poor carrier separation in phosphorus and the lack of visible light absorption in TiO_2. Further, black P@TiO_2 does not show a noticeable increase in photocurrent density which can be attributed to the lack of a synergistic photocatalytic process which is likely due to the higher degree of oxidation of P in black P to P_xO_y which was evident in XPS data (Figure S5). Interestingly, the fibrous

red P@TiO_2-hybrid exhibited a relatively high photocurrent density (0.60 mA cm^{-2}) suggesting successful formation of heterojunction and better charge transfer between fibrous red P to TiO_2 (Figure 8a). The viability of the photocatalytic system to perform under visible light was tested by irradiating the specimens with 425 nm LED light and a power density of 54.15 mA cm^{-2}. The increase in photocurrent under 425 nm irradiation clearly demonstrates the applicability of the system to perform at longer wavelengths (Figure S7). The highest applied bias photon-to-current efficiency percentage (ABPE%, calculation details are given in the Supporting Information) was found for fibrous red P@TiO_2 nanohybrid which was approximately 3.5 times higher than for TiO_2 and pristine fibrous red P which demonstrates that heterojunction formation with TiO_2 increases the photo-electrocatalytic performance significantly (Figure 8d).[56-57]

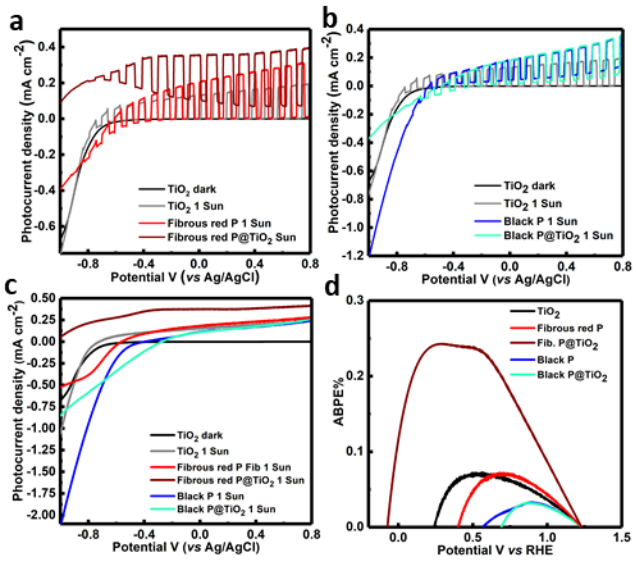

Figure 8. a), **b)** and Linear sweep voltammogram of TiO_2, fibrous red P, fibrous red P@TiO_2, black P, black P@TiO_2, under dark condition, and under 1 solar simulated AM1.5 G light irradiation (100 mW cm^{-2}) showing photo response during On-Off and **c)** standard mode cycling. **d)** ABPE % *vs* RHE plot under AM1.5 G light irradiation (100 mW cm^{-2}) Color: TiO_2 under dark (black), TiO_2 under AM1.5 G (black), fibrous red P (red), fibrous red P@TiO_2 (brown), black P (blue) and black P@TiO_2 (light blue).

The band edge energies with respect to vacuum level of all samples were determined from work function (WF) and valence band (VB) spectra acquired using ultraviolet photoelectron spectroscopy (UPS) (Figure 9). The WF was calculated by subtracting the energy of emitted secondary electrons ($E_{cut\text{-}off}$) from the energy of incident UV light (He laser: 21.21 eV) using the following expression WF (Φ) = 21.21-$E_{cut\text{-}off}$. The extrapolation of the linear region of the WF spectrum on X and Y scale and their point of intersection gave the value of the cut-off energy. The $E_{cut\text{-}off}$ energies of TiO_2, fibrous red P@TiO_2, and black P@TiO_2 were found to be 16.40, 16.24 and 16.11 eV respectively. Hence, the values of WF were calculated to be 4.81, 4.97 and 5.10 eV (Figure 9a and c and insets). The increase of WF value demonstrates depletion region formation with concomitant band bending at the solid-state hetero-interface which leads to deepening of the Fermi level of TiO_2 in P@TiO_2 hybrids. Additionally, the valence band maximum (VB_{max}) values calculated *via* linear extrapolation of the leading edges of UPS valence band spectra for fibrous red P, fibrous red P@TiO_2 black P and black P@TiO_2, were found to be 0.82, 1.49 1.41 and 1.45 eV below the Fermi level. The small difference between Fermi level and valence band ($E_F - E_{VBmax}$) for fibrous red P (0.82 eV) and black P (1.41 eV) reveals, that the Fermi level was close to VB_{max} and the samples were moderately *p*-type. Further, XPS valence band spectra of TiO_2 gave the value of VB_{max} to be 3.15 eV below the Fermi level (Figure S4) The increase in VB_{max} in black P@TiO_2 and fibrous red P@TiO_2 implies slightly uplifted Fermi level of phosphorus in the heterojunction during Fermi level alignment and band bending (Figure 10). From WF and VB_{max} results, it can be concluded that heterojunction formation between phosphorus and TiO_2 was facilitated by upward band

bending in TiO_2 and downward band bending in phosphorus allotropes (black P and fibrous red P) as expected for a *p-n* heterojunction.

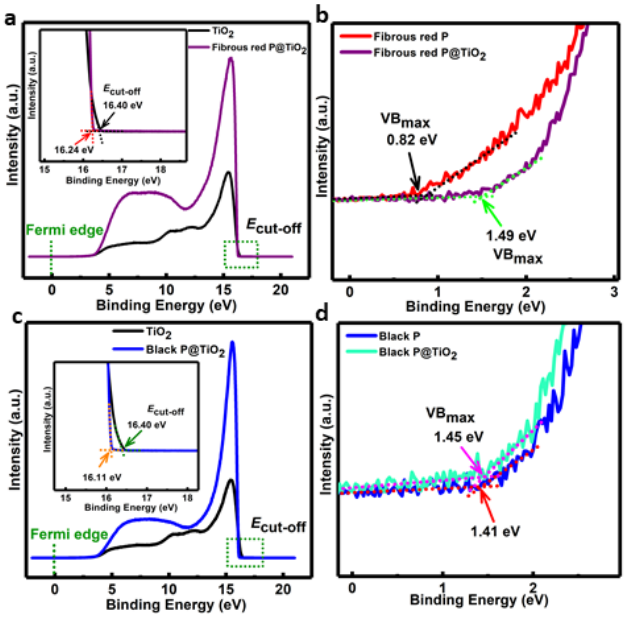

Figure 9. UPS work function spectra of **a)** TiO_2 and fibrous red P@TiO_2 and **c)** TiO_2 and black P@TiO_2 and Inset showing cut-off energy ($E_{cut\text{-}off}$). The value of Work function (WF) was determined from the UPS work function spectra by using the equation WF (Φ) = 21.21 – $E_{cut\text{-}off}$, where 21.21 eV is the energy of the incident He laser used for UPS. UPS valence band spectra of **b)** Fibrous red P and fibrous red P@TiO_2, and **d)** black P and black P@TiO_2 Color: TiO_2 (black), fibrous red P (red), fibrous red P@TiO_2 (purple), black P (blue) and black P@TiO_2 (light blue).

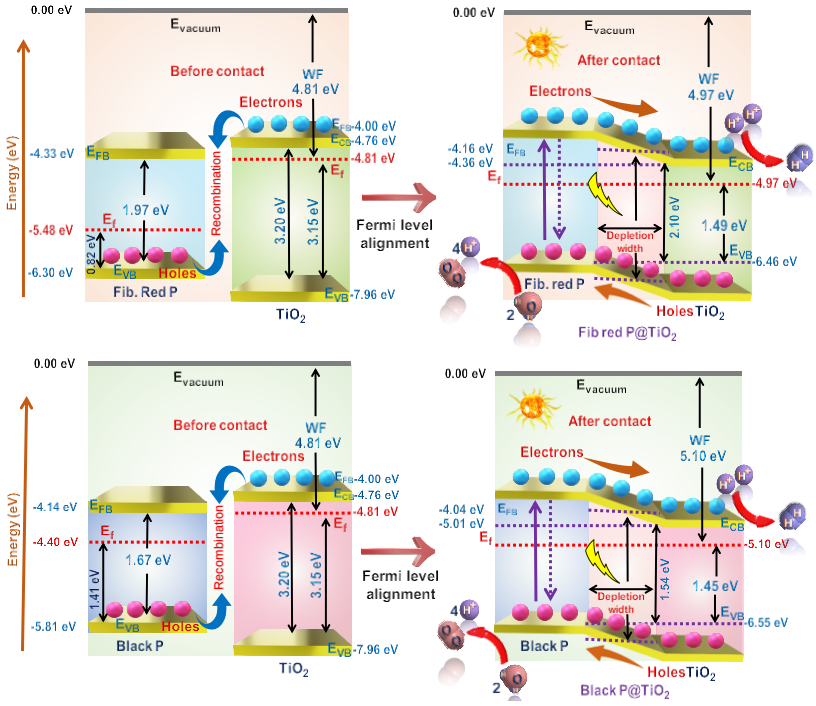

Figure 10. Energy level diagrams illustrating plausible charge separation mechanism in phosphorus allotrope@TiO_2

Plausible mechanism

The water splitting process proceeds *via* absorption of light by the semiconductors, generating electron hole pairs which drive proton reduction- and water oxidation reactions. In photoelectrochemical water splitting, electrons in the conduction band CB of semiconductors move toward the Pt-cathode where they reduce protons while holes in the valence band VB of the semiconductors oxidize water to produce oxygen at the anode. Wide band gap (>1.23 eV) and aligned position of conduction and valence band (CB<0.00 eV and VB>+1.23 eV *vs* NHE at pH-0) are required to achieve proton reduction and water oxidation, respectively. TiO_2 has a large band gap and electron hole pairs can only be produced under UV-irradiation which demonstrates the origin of very small

photocurrent density in LSV. However, from DR UV-Vis the value of the optical band gap was found to be 2.97 eV which corresponds to 417 nm – in other words, a small visible light fraction can be absorbed by TiO_2. The decrease in band gap of TiO_2 might be explained due to a presence of few Ti^{3+} defects, oxygen vacancy and trap sites. Moreover because of the low band gaps of pristine black P and fibrous red P, generating sufficient reductive and oxidative electron and holes to facilitate water splitting reaction can be affected.[58-59] However, a hybrid material, consisting of fibrous red P with TiO_2 was found to be an efficient photocatalyst as a result of the formation of a heterojunction and efficient charge transfer between fibrous red P and TiO_2. The heterojunction formation leads to Fermi level alignment. During Fermi level alignment electrons flow from one semiconductor to another which equilibrates Fermi level position between the semiconductors. Measurements of the flat band potential for TiO_2, pristine fibrous red P and black P were carried out via Mott Schottky analysis (Figure S8b), and found to be -0.70, -0.37 and-0.56 V *vs* Ag/AgCl (-4.00, -4.14, -4.33 eV on $E_{vac.}$ scale). This indicates an electron transfer from TiO_2 to black P or fibrous red P, respectively during Fermi level alignment. After hybrid heterojunction formation and reaching equilibrium, the position of flat band potential of fibrous red P@TiO_2 and black P@TiO_2 was found to be -0.54 and -0.66 V *vs* Ag/AgCl (-4.16 and -4.04 eV at E_{vac} scale) (Figure 10). The down-shifting of flat band potential of TiO_2 in hybrid systems suggest downward band bending of the conduction band edge of fibrous red and black P while upward band bending in TiO_2 occurs. This clearly demonstrate formation of *p-n* type heterojunction between phosphorus allotropes and TiO_2. These observations were also supported by WF values (position of Fermi level in vacuum) where WF of TiO_2 changed from 4.97 *vs* vacuum in fibrous red P@TiO_2 while

4.81 to 5.10 eV in black P@TiO_2 (Figure 10). The increase in WF value in hybrid materials demonstrates lower shifting of the Fermi level which agrees well with heterojunction formation.

Additionally, a deeper VB_{max} in hybrid phosphorus allotrope@TiO_2 compounds than in pristine phosphorus allotropes suggest successful formation of heterojunction and generation of more oxidative holes to facilitate water splitting. Based on above findings we have sketched a band structure diagram of the hybrid materials which demonstrates that more efficient water splitting was possible due to *p-n* heterojunction formation and better charge separation, Figure 10). Further, Nyquist plots demonstrate that charge transfer resistance and charge transport resistance of hybrids were lower in comparison to pristine TiO_2 which suggest better charge transfer and transport in hybrid materials (Figure S8). The cavities of the TiO_2 nanotube membranes are evidently filled with visible light absorbing phosphorus allotropes. Thus, generated electron hole pairs can be transferred to TiO_2. Due to a short path distance and TiO_2 exhibiting a high carrier mobility, carrier recombination can be prevented and a fast transit of the charge carriers towards the semiconductor-electrolyte interface is enabled.

CONCLUSION

Hybrid heterojunction systems for optoelectronic applications were designed, fabricated, characterized and tested. The so-called mineralization principle for short way gas phase transport of solids was performed to grow semiconductors on TiO_2 nanotube arrays. Fibrous red phosphorus and black phosphorus were successfully deposited onto and into electrochemically produced TiO_2 nanotube membranes. The formation of hybrid

nanostructures was analysed with several spectroscopic and diffraction methods such as XRD, EDX-analysis, STEM analysis, Raman spectroscopy, UV-vis- and XPS analysis. The effectiveness of the vapor transport was verified through SEM, STEM, elemental mapping of surface and cross section of nanohybrids, showing a deposition of the materials inside the tubes.

Raman spectra taken at the surface and along the razor-cut cross section of the nanotubes confirmed the penetration and growth of fibrous red P up to 15 µm (65 µm in length) and black P up to 7 µm into the nanotubes (60 µm in length). The fibrous red P@TiO_2 and black P@TiO_2 hybrid materials displayed improved photoelectrochemical performance for water splitting in the visible light regime due to successful *p-n* heterojunction formation. UPS WF spectra demonstrate band alignment, the Fermi level of TiO_2 gets downshifted while an upshift was observed for the phosphorous allotropes during heterojunction formation. This formation enables a carrier transportation from the VB of downshifted TiO_2 to phosphorus allotropes resulting in a successful oxidation in water splitting. At the same time, Mott-Schottky plots corroborate the occurrence of more reductive flat bands in hybrid phosphorus allotrope@TiO_2 materials which facilitate effective reduction of hydrogen. The increased charge carrier mobility, lower charge transfer resistance, and lower charge transport resistance of such hybrid materials leads to better charge separation and improved photoelectrochemical performance.

Supporting Information. Experimental details on synthesis, physicochemical and photoelectrochemical characterization. Additional characterization on Powder-XRD, Raman analysis, EDS analysis, DRS UV-Vis, HR-XPS, photocurrent density, EIS characterization and Nyquist plots, Mott-Schottky plots, XPS valence band spectra.

Author Contributions

EÜ and RK did synthesis and characterization of phosphorus/hybrid materials. Pawan Kumar was involved in XPS, UPS, and photoelectrochemical studies and compilating the results. Piyush Kar performed electrochemical characterizations. KS and TN planned and supervised the research. All authors were involved in writing their respective parts.

ACKNOWLEDGMENT

This work has been performed as part of the international graduate school ATUMS (IRTG 2022) funded by the DFG and NSERC. The performance and assistance of STEM-EDX by Peng Li, Shihong Xu and Anqiang He from nanoFAB at the University of Alberta is gratefully acknowledged. We like to thank Anna Vogel for Raman spectroscopy of the samples. KS acknowledges Natural Sciences and Engineering Research Council of Canada (NSERC), the National Research Council Canada (NRC), Future Energy Systems (FES) and CMC Microsystems for research funding and allowance for tool usages. Pawan Kumar is thankful to Future Energy System for the postdoctoral research fellowship. We kindly acknowledge Dr. Kazi Alam for DR UV-Vis measurements.

ABBREVIATIONS

Fib. P, fibrous red P; fibrous red P@TiO_2, hybrid of fibrous red P and TiO_2; black P@TiO_2, hybrid of black P and TiO_2, Scanning electron microscopy; SEM; STEM-EDS, Scanning transmission electron microscope-Energy dispersive X-ray spectroscopy; XRD, X-ray diffraction; XPS, X-ray photoelectron spectroscopy; DR UV-Vis, Diffuse reflectance Ultraviolet-visible spectroscopy; NHE, normal hydrogen electrode; IR, Infrared radiation; WF, work function; VB, valence band; UPS, Ultraviolet photoelectron spectroscopy; LSV, Linear sweep voltammetry; FTO, Fluorine-doped tin oxide.

REFERENCES

1. Yuan, Y.-P.; Ruan, L.-W.; Barber, J.; Joachim Loo, S. C.; Xue, C., Hetero-nanostructured suspended photocatalysts for solar-to-fuel conversion. *Energy Environ. Sci.* **2014,** *7* (12), 3934-3951.

2. Liao, L.; Su, Z.; Wang, Y.; Li, Y.; Lu, X.; Zhang, Q.; Zhao, Z.; Wei, D.; Feng, G.; Yu, Q.; Cai, X.; Baldelli, S.; Zhao, J.; Ren, Z.; Fang, H.; Robles-Hernandez, F.; Bao, J., Efficient solar water-splitting using a nanocrystalline CoO photocatalyst. *Nat Nanotechnol.* **2014,** *9* (1), 69-73.

3. Liu, J.; Liu, Y.; Liu, N.; Han, Y.; Zhang, X.; Huang, H.; Lifshitz, Y.; Lee, S.-T.; Zhong, J.; Kang, Z., Metal-free efficient photocatalyst for stable visible water splitting via a two-electron pathway. *Science* **2015,** *347* (6225), 970-974.

4. Roger, I.; Shipman, M. A.; Symes, M. D., Earth-abundant catalysts for electrochemical and photoelectrochemical water splitting. *Nat. Rev. Chem.* **2017,** *1* (1), 0003.

5. Maeda, K.; Teramura, K.; Lu, D.; Takata, T.; Saito, N.; Inoue, Y.; Domen, K., Photocatalyst releasing hydrogen from water. *Nature* **2006,** *440* (7082), 295.

6. Sun, Y.; Cheng, H.; Gao, S.; Sun, Z.; Liu, Q.; Liu, Q.; Lei, F.; Yao, T.; He, J.; Wei, S., Freestanding tin disulfide single-layers realizing efficient visible-light water splitting. *Angew. Chem.* **2012,** *124* (35), 8857-8861.

7. Wang, Q.; Hisatomi, T.; Jia, Q.; Tokudome, H.; Zhong, M.; Wang, C.; Pan, Z.; Takata, T.; Nakabayashi, M.; Shibata, N., Scalable water splitting on particulate photocatalyst sheets with a solar-to-hydrogen energy conversion efficiency exceeding 1%. *Nat. Mater.* **2016,** *15* (6), 611.

8. Habisreutinger, S. N.; Schmidt-Mende, L.; Stolarczyk, J. K., Photocatalytic reduction of CO_2 on TiO_2 and other semiconductors. *Angew. Chem. Int. Ed.* **2013,** *52* (29), 7372-7408.

9. Sheridan, M. V.; Hill, D. J.; Sherman, B. D.; Wang, D.; Marquard, S. L.; Wee, K.-R.; Cahoon, J. F.; Meyer, T. J., All-in-One Derivatized Tandem p+n-Silicon–SnO_2/TiO_2 Water Splitting Photoelectrochemical Cell. *Nano Lett.* **2017,** *17* (4), 2440-2446.

10. Moniz, S. J.; Shevlin, S. A.; Martin, D. J.; Guo, Z.-X.; Tang, J., Visible-light driven heterojunction photocatalysts for water splitting–a critical review. *Energy Environ. Sci.* **2015,** *8* (3), 731-759.

11. Jaafar, S. N. H.; Minggu, L. J.; Arifin, K.; Kassim, M. B.; Wan, W. R. D., Natural dyes as TiO_2 sensitizers with membranes for photoelectrochemical water splitting: An overview. *Renewable Sustainable Energy Rev.* **2017,** *78*, 698-709.

12. Ge, M.; Li, Q.; Cao, C.; Huang, J.; Li, S.; Zhang, S.; Zhang, K.; Lai, Y.; Chen, Z.; Al-Deyab, S. S., One-dimensional TiO_2 Nanotube Photocatalysts for Solar Water Splitting. *Adv. Sci.* **2017,** *4* (1), 1600152.

13. Park, J. H.; Kim, S.; Bard, A. J., Novel carbon-doped TiO_2 nanotube arrays with high aspect ratios for efficient solar water splitting. *Nano Lett.* **2006,** *6* (1), 24-28.

14. Pu, Y.-C.; Wang, G.; Chang, K.-D.; Ling, Y.; Lin, Y.-K.; Fitzmorris, B. C.; Liu, C.-M.; Lu, X.; Tong, Y.; Zhang, J. Z., Au nanostructure-decorated TiO_2 nanowires exhibiting photoactivity across entire UV-visible region for photoelectrochemical water splitting. *Nano Lett.* **2013,** *13* (8), 3817-3823.

15. Lee, C. Y.; Taylor, A. C.; Beirne, S.; Wallace, G. G., 3D-Printed Conical Arrays of TiO_2 Electrodes for Enhanced Photoelectrochemical Water Splitting. *Adv. Energy Mater.* **2017,** *7* (21), 1701060.

16. de Brito, J. F.; Tavella, F.; Genovese, C.; Ampelli, C.; Zanoni, M. V. B.; Centi, G.; Perathoner, S., Role of CuO in the modification of the photocatalytic water splitting behavior of TiO_2 nanotube thin films. *Appl. Catal., B* **2018,** *224*, 136-145.

17. Ning, X.; Li, J.; Yang, B.; Zhen, W.; Li, Z.; Tian, B.; Lu, G., Inhibition of photocorrosion of CdS via assembling with thin film TiO_2 and removing formed oxygen by artificial gill for visible light overall water splitting. *Appl. Catal., B* **2017,** *212*, 129-139.

18. Mor, G. K.; Shankar, K.; Paulose, M.; Varghese, O. K.; Grimes, C. A., Use of highly-ordered TiO_2 nanotube arrays in dye-sensitized solar cells. *Nano Lett.* **2006,** *6* (2), 215-218.

19. Mor, G. K.; Varghese, O. K.; Paulose, M.; Shankar, K.; Grimes, C. A., A review on highly ordered, vertically oriented TiO_2 nanotube arrays: Fabrication, material properties, and solar energy applications. *Sol. Energy Mater. Sol. Cells* **2006,** *90* (14), 2011-2075.

20. Wang, F.; Ng, W. K. H.; Jimmy, C. Y.; Zhu, H.; Li, C.; Zhang, L.; Liu, Z.; Li, Q., Red phosphorus: an elemental photocatalyst for hydrogen formation from water. *Appl. Catal., B* **2012,** *111*, 409-414.

21. Kudo, A.; Miseki, Y., Heterogeneous photocatalyst materials for water splitting. *Chem. Soc. Rev.* **2009,** *38* (1), 253-278.

22. Roy, P.; Berger, S.; Schmuki, P., TiO_2 nanotubes: synthesis and applications. *Angew. Chem. Int. Ed.* **2011,** *50* (13), 2904-2939.

23. Schock, H.; Meissner, D., Solarzellen-Physikalische Grundlagen und Anwendungen in der Photovoltaik. *Vieweg & Sohn: Wiesbaden* **1993**.

24. Regonini, D.; Bowen, C. R.; Jaroenworaluck, A.; Stevens, R., A review of growth mechanism, structure and crystallinity of anodized TiO_2 nanotubes. *Mater. Sci. Eng., R* **2013,** *74* (12), 377-406.

25. Hahn, R.; Macak, J.; Schmuki, P., Rapid anodic growth of TiO_2 and WO_3 nanotubes in fluoride free electrolytes. *Electrochem. Commun.* **2007,** *9* (5), 947-952.

26. Ravi, P.; Rao, V. N.; Shankar, M.; Sathish, M., $CuOCr_2O_3$ core-shell structured co-catalysts on TiO_2 for efficient photocatalytic water splitting using direct solar light. *Int. J. Hydrogen Energy* **2018,** *43* (8), 3976-3987.

27. Keyes, R. W., The electrical properties of black phosphorus. *Phys. Rev.* **1953,** *92* (3), 580.

28. Morita, A., Semiconducting black phosphorus. *Appl. Phys. A* **1986,** *39* (4), 227-242.

29. Yan, J.; Ji, Y.; Kong, L.; Li, Y.; Navlani-García, M.; Liu, S.; Kuwahara, Y.; Mori, K.; Che, M.; Yamashita, H., Black Phosphorus-Based Compound with Few Layers for Photocatalytic Water Oxidation. *ChemCatChem* **2018,** *10* (16), 3424-3428.

30. Li, L.; Yu, Y.; Ye, G. J.; Ge, Q.; Ou, X.; Wu, H.; Feng, D.; Chen, X. H.; Zhang, Y., Black phosphorus field-effect transistors. *Nat. Nanotechnol.* **2014,** *9* (5), 372.

31. Yuan, H.; Liu, X.; Afshinmanesh, F.; Li, W.; Xu, G.; Sun, J.; Lian, B.; Curto, A. G.; Ye, G.; Hikita, Y., Polarization-sensitive broadband photodetector using a black phosphorus vertical p–n junction. *Nat. Nanotechnol.* **2015,** *10* (8), 707.

32. Viti, L.; Hu, J.; Coquillat, D.; Knap, W.; Tredicucci, A.; Politano, A.; Vitiello, M. S., Black-phosphorus Terahertz photodetectors. *arXiv preprint arXiv:1805.00735* **2018**.

33. Zhou, Y.; Zhang, Y.; Lin, M.; Long, J.; Zhang, Z.; Lin, H.; Wu, J. C.-S.; Wang, X., Monolayered Bi_2WO_6 nanosheets mimicking heterojunction interface with open surfaces for photocatalysis. *Nat. Commun.* **2015,** *6*, 8340.

34. Chen, S.; Qi, Y.; Hisatomi, T.; Ding, Q.; Asai, T.; Li, Z.; Ma, S. S. K.; Zhang, F.; Domen, K.; Li, C., Efficient Visible Light-Driven Z-Scheme Overall Water Splitting Using a $MgTa_2O_6$−xNy/TaON Heterostructure Photocatalyst for H_2 Evolution. *Angew. Chem.* **2015,** *127* (29), 8618-8621.

35. Shang, L.; Tong, B.; Yu, H.; Waterhouse, G. I.; Zhou, C.; Zhao, Y.; Tahir, M.; Wu, L. Z.; Tung, C. H.; Zhang, T., Hydrogen Evolution: CdS Nanoparticle-Decorated Cd Nanosheets for Efficient Visible Light-Driven Photocatalytic Hydrogen Evolution, Adv. Energy Mater. **2016,** *6* (3).

36. Nguyen, C. C.; Vu, N. N.; Do, T.-O., Recent advances in the development of sunlight-driven hollow structure photocatalysts and their applications. *J. Mater. Chem. A* **2015,** *3* (36), 18345-18359.

37. Lewis, N. S., Toward cost-effective solar energy use. *Science* **2007,** *315* (5813), 798-801.

38. Zhang, X.; Han, F.; Shi, B.; Farsinezhad, S.; Dechaine, G. P.; Shankar, K., Photocatalytic conversion of diluted CO_2 into light hydrocarbons using periodically modulated multiwalled nanotube arrays. *Angew. Chem. Int. Ed.* **2012,** *51* (51), 12732-12735.

39. Mohammadpour, A.; Kar, P.; D Wiltshire, B.; M Askar, A.; Shankar, K., Electron transport, trapping and recombination in anodic TiO_2 nanotube arrays. *Curr. Nanosci.* **2015,** *11* (5), 593-614.

40. Macak, J.; Barczuk, P.; Tsuchiya, H.; Nowakowska, M.; Ghicov, A.; Chojak, M.; Bauer, S.; Virtanen, S.; Kulesza, P.; Schmuki, P., Self-organized nanotubular TiO_2 matrix as support for dispersed Pt/Ru nanoparticles: Enhancement of the electrocatalytic oxidation of methanol. *Electrochem. Commun.* **2005,** *7* (12), 1417-1422.

41. Paramasivam, I.; Macak, J.; Ghicov, A.; Schmuki, P., Enhanced photochromism of Ag loaded self-organized TiO_2 nanotube layers. *Chem. Phys. Lett.* **2007,** *445* (4-6), 233-237.

42. Yang, G.; Chen, D.; Ding, H.; Feng, J.; Zhang, J. Z.; Zhu, Y.; Hamid, S.; Bahnemann, D. W., Well-designed 3D $ZnIn_2S_4$ nanosheets/TiO_2 nanobelts as direct Z-scheme photocatalysts for CO_2 photoreduction into renewable hydrocarbon fuel with high efficiency. *Appl. Catal., B* **2017,** *219*, 611-618.

43. Zhou, D.; Chen, Z.; Yang, Q.; Shen, C.; Tang, G.; Zhao, S.; Zhang, J.; Chen, D.; Wei, Q.; Dong, X., Facile Construction of g-C_3N_4 Nanosheets/TiO_2 Nanotube Arrays as Z-Scheme Photocatalyst with Enhanced Visible-Light Performance. *ChemCatChem* **2016,** *8* (19), 3064-3073.

44. Pi, Y.; Li, Z.; Xu, D.; Liu, J.; Li, Y.; Zhang, F.; Zhang, G.; Peng, W.; Fan, X., 1T-Phase MoS_2 Nanosheets on TiO_2 Nanorod Arrays: 3D Photoanode with Extraordinary Catalytic Performance. *ACS Sustainable Chem. Eng.* **2017,** *5* (6), 5175-5182.

45. Qin, P.; Paulose, M.; Dar, M. I.; Moehl, T.; Arora, N.; Gao, P.; Varghese, O. K.; Grätzel, M.; Nazeeruddin, M. K., Stable and efficient perovskite solar cells based on titania nanotube arrays. *Small* **2015,** *11* (41), 5533-5539.

46. Thakur, U.; Kisslinger, R.; Shankar, K., One-dimensional electron transport layers for perovskite solar cells. *Nanomaterials* **2017,** *7* (5), 95.

47. Lou, Z.; Li, F.; Deng, J.; Wang, L.; Zhang, T., Branch-like hierarchical heterostructure (α-Fe_2O_3/TiO_2): a novel sensing material for trimethylamine gas sensor. *ACS Appl. Mater. Interfaces* **2013,** *5* (23), 12310-12316.

48. Eckstein, N.; Hohmann, A.; Weihrich, R.; Nilges, T.; Schmidt, P., Synthesis and Phase Relations of Single-Phase Fibrous Phosphorus. *Z. Anorg. Allg. Chem.* **2013,** *639* (15), 2741-2743.

49. Grotz, C.; Köpf, M.; Baumgartner, M.; Jantke, L. A.; Raudaschl-Sieber, G.; Fässler, T. F.; Nilges, T., Synthesis, Structure, and Properties of NaP_7, a Phosphorus-rich Polyphosphide. *Z. Anorg. Allg. Chem.* **2015,** *641* (8-9), 1395-1399.

50. Pfister, D.; Schaefer, K.; Ott, C.; Gerke, B.; Poettgen, R.; Janka, O.; Baumgartner, M.; Efimova, A.; Hohmann, A.; Schmidt, P.; Venkatachalam, S.; van Wuellen, L.; Schuermann, U.; Kienle, L.; Duppel, V.; Parzinger, E.; Miller, B.; Becker, J.; Holleitner, A.; Weihrich, R.; Nilges, T., Inorganic Double Helices in Semiconducting SnIP. *Adv. Mater.* **2016,** *28* (44), 9783-9791.

51. Castellanos-Gomez, A., Black phosphorus: narrow gap, wide applications. *J. Phys. Chem. Lett.* **2015,** *6* (21), 4280-4291.

52. Abbas, A. N.; Liu, B.; Chen, L.; Ma, Y.; Cong, S.; Aroonyadet, N.; Köpf, M.; Nilges, T.; Zhou, C., Black phosphorus gas sensors. *ACS nano* **2015,** *9* (5), 5618-5624.

53. Grätzel, M., Photoelectrochemical cells. *Nature* **2001,** *414* (6861), 338.

54. Guo, Z.; Zhang, H.; Lu, S.; Wang, Z.; Tang, S.; Shao, J.; Sun, Z.; Xie, H.; Wang, H.; Yu, X. F., From black phosphorus to phosphorene: basic solvent exfoliation, evolution of Raman scattering, and applications to ultrafast photonics. *Adv. Funct. Mater.* **2015,** *25* (45), 6996-7002.

55. Wang, H.; Yang, X.; Shao, W.; Chen, S.; Xie, J.; Zhang, X.; Wang, J.; Xie, Y., Ultrathin black phosphorus nanosheets for efficient singlet oxygen generation. *J. Am. Chem. Soc.* **2015,** *137* (35), 11376-11382.

56. Chen, Z.; Dinh, H. N.; Miller, E., *Photoelectrochemical water splitting*. Springer: 2013.

57. Zhang, X.; Zhang, B.; Cao, K.; Brillet, J.; Chen, J.; Wang, M.; Shen, Y., A perovskite solar cell-TiO_2@$BiVO_4$ photoelectrochemical system for direct solar water splitting. *J. Mater. Chem. A* **2015,** *3* (43), 21630-21636.

58. Hoang, S.; Berglund, S. P.; Hahn, N. T.; Bard, A. J.; Mullins, C. B., Enhancing visible light photo-oxidation of water with TiO_2 nanowire arrays via cotreatment with H_2 and NH_3: synergistic effects between Ti^{3+} and N. *J. Am. Chem. Soc.* **2012,** *134* (8), 3659-3662.

59. Chen, X.; Liu, L.; Peter, Y. Y.; Mao, S. S., Increasing solar absorption for photocatalysis with black hydrogenated titanium dioxide nanocrystals. *Science* **2011**, 1200448.

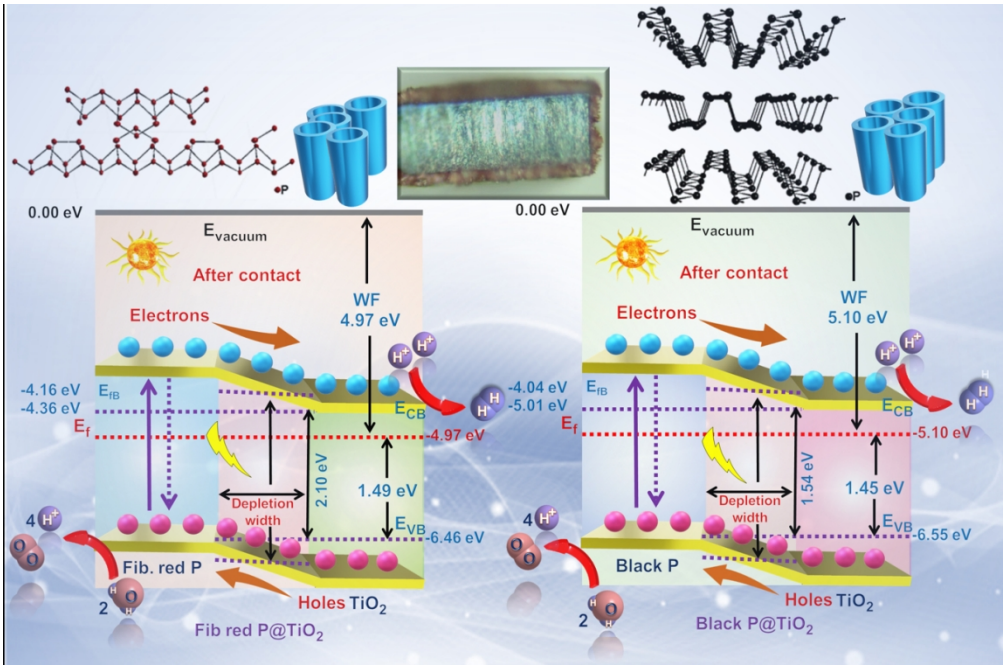

Phosphorus allotrope@TiO_2 membranes and charge separation mechanism

231x152mm (149 x 149 DPI)